Supporting Information

Interfacial defect engineering to boost deep-ultraviolet photodetection based on a wide bandgap semiconductor heterostructure

Han Wu,[1] Lincong Shu,[2] Sihan Yan,[2] Shulin Sha,[4] Qinghua Zhang,[5] Zeng Liu,[3] Shan Li,[2] Weihua Tang,[2] Yuehui Wang,[7] Jiaying Shen,[6] Zhenping Wu,[6] Kun Lin,[1] Qiang Li,[1] Jun Miao,[1] Xianran Xing[1,*]

[1] *Beijing Advanced Innovation Center for Materials Genome Engineering, Institute of Solid State Chemistry, University of Science and Technology Beijing, Beijing 100083, China*

[2] *College of Integrated Circuit Science and Engineering, Nanjing University of Posts and Telecommunications, Nanjing 210023, China*

[3] *School of Electronic Information Engineering, Inner Mongolia University, Hohhot 010021, China*

[4] *College of Physics, MIIT Key Laboratory of Aerospace Information Materials and Physics, Key Laboratory for Intelligent Nano Materials and Devices, Nanjing University of Aeronautics and Astronautics, No. 29 Jiangjun Road, Nanjing 211106, China*

[5] *Beijing National Laboratory for Condensed Matter Physics, Institute of Physics, Chinese Academy of Sciences, Beijing 100190, China.*

[6] *State Key Laboratory of Information Photonics and Optical Communications & School of Science, Beijing University of Posts and Telecommunications, Beijing 100876, China*

[7] *Key Laboratory for the Physics and Chemistry of Nanodevices and Center for Carbon-based Electronics, School of Electronics, Peking University, Beijing, China*

**Corresponding author: xing@ustb.edu.cn.*

Han Wu, Lincong Shu and Sihan Yan contributed equally to the manuscript

Experimental Section

Film growth and device fabrication

The In_2O_3 and Ga_2O_3 layers were sequentially grown by PLD on (111)-YSZ substrates. The In_2O_3 and Ga_2O_3 were grown at 750 °C in oxygen partial pressure of 26 Pa and 750 °C in oxygen partial pressure of 5 pa, respectively. A KrF excimer laser with a wavelength of 248 nm was used with laser fluence of 1.5 J cm^{-2} and repetition rate of 4 Hz for all the layers. After the deposition of In_2O_3 layer, the chamber was evacuated to around $1x10^{-4}$ pa and maintained for 180 minutes to create a certain amount of oxygen vacancies on the surface of In_2O_3 layer. The films was cooled down to room temperature at a rate of 10 °C min^{-1} under an oxygen pressure of 100 torr, after all deposition was completed. 30-μm-diameter Au/Ti top electrodes (100 nm/5 nm) were deposited on the surface of samples by electron beam evaporation. The electrodes were patterned by photolithography, and the area was accurately determined.

Material characterizations and photoresponse measurements

The crystal structure of the thin films was analyzed by means of X-ray diffraction (XRD) at Beijing Synchrotron Radiation Facility (1W1A beamline, China) using high-resolution synchrotron X-rays. For the distinguished diffracted intensity, the In_2O_3/Ga_2O_3 heterostructure for the x-ray diffraction measurements were 10 nm/40 nm, respectively. The surface morphologies were examined on a commercial multifunction AFM instrument (Asylum Research MFP-3D Infinite) with tapping mode. X-ray photoelectron spectrum was obtained with an AXIS $ULTRA^{DLD}$ (Kratos, Japan) instrument equipped with an electron flood and scanning ion gun. A Lambda 1050 UV/Vis/NIR spectrophotometer was used to record the absorption spectra. The Hall measurements of In_2O_3 layers were carried out with a six-port Hall bar configuration by a Physical Properties Measurement System instrument (PPMS, Quantum Design). On account of the sheet resistance of 5-nm-thickness In_2O_3 over the test limit of PPMS, the In_2O_3 layers for the Hall measurements were 10 nm. The photoresponse I-V and I-T curves under varying irradiation intensities at the wavelength of 254 nm were

recorded by an Agilent-B1500A semiconductor analyzer connected to a probe station using triaxial cables to ensure low-noise measurements. The transient response measurements were accessed using a Nd:YAG pulsed laser (Ekspla, NT342) and a digital oscilloscope (Tektronix, MSO54).

Electron microscopy and EDS

Electron microscopy and EDS were performed on two spherical-aberration-corrected TEM instruments (Titan G2 80-200 ChemiSTEM, FEI; and ARM200F, JEOL) operated at 200 kV equipped with a Super-X EDS detector. Atomic-resolution imaging was performed in the HAADF-STEM mode, where the intensity in the image is ~Z^2, thus yielding a clear atomic number contrast. Images were analyzed using specific analysis software. EDS was performed simultaneously with image acquisition in the HAADF-STEM mode. Chemical maps were acquired for 20 min with conditions optimized and collected at thousands of X-ray photons per second, and analyzed using Bruker Espirit software.

Hall formula derivation

The In_2O_3 layer was etched into six-port Hall bar devices as shown in supplementary Figure S1. The Hall mobility and carrier density are determined by Hall effect and given by the following expression,

$$R_{XY} = \frac{B}{n_H e d} \quad (1)$$

$$\frac{R_{XY}}{R_{XX}} = \frac{\mu_H b B}{L} \quad (2)$$

where the d is the thickness of the channel, b is the width of the channel, L is the length of the channel, B is the magnetic field strength, e is the electron charge ($e=1.602\times10^{-19}$ C), n_H is the carrier density, μ_H is the Hall mobility, R_{XY} and R_{XX} are the resistance along the channel width and length, respectively.

Energy band alignments derivation

XPS scan was used to quantitatively determine the energy band alignments of the heterostructure. Four samples: In_2O_3 (100 nm), Ga_2O_3 (100 nm)/In_2O_3 (5 nm), and ultrathin Ga_2O_3 (2 nm)/In_2O_3 (5 nm) were fabricated using the same growth conditions. Kraut's method was employed to calculate the valence band offset (ΔE_V) and conduction band offset (ΔE_C) by using the following equations:[1]

$$\Delta E_{V-Ga_2O_3/In_2O_3} = \left(E_{Ga-core}^{Ga_2O_3} - E_{VBM}^{Ga_2O_3}\right) - \left(E_{In-core}^{In_2O_3} - E_{VBM}^{In_2O_3}\right) - \left(E_{Ga-core}^{Ga_2O_3/In_2O_3} - E_{In-core}^{Ga_2O_3/In_2O_3}\right)$$

Where $E_{Ga-core}^{Ga_2O_3}$, $E_{In-core}^{In_2O_3}$, $E_{VBM}^{Ga_2O_3}$ and $E_{VBM}^{In_2O_3}$ are the core levels of Ga 3d, In 3d, and binding energy of the VBM for Ga_2O_3 (100 nm)/In_2O_3 (5 nm) samples and In_2O_3 (100 nm)samples, respectively. $E_{Ga-core}^{Ga_2O_3/In_2O_3}$ and $E_{In-core}^{Ga_2O_3/In_2O_3}$ are the core levels of Ga 3d and In 3d for the Ga_2O_3 (2 nm)/In_2O_3 (5 nm) samples. Hence, the ΔE_V for Ga_2O_3/ In_2O_3 is 1.55 eV. Given the respective bandgaps for Ga_2O_3 (4.95 eV) and In_2O_3 (3.31 eV) obtained in Figure S8b and S8c, the conduction band minimum (CBM) for the heterostructure could be consequently determined. The obtained values of ΔE_C for Ga_2O_3/ In_2O_3 are 0.09 eV.

DFT methods

The DS-PAW package was utilized for high-precision geometry optimization of In_2O_3. In this process, the projected augmented wave (PAW) method combined with the Perdew-Burke-Ernzerhof (PBE) exchange-correlation functional was employed to obtain the electronic ground state. The electron energy convergence for the electronic structure was set to $1E^{-4}$ eV, and the atomic force convergence was set to 0.01 eV/Å. A 7×7×7 k-point mesh was used to render the accuracy of the optimized geometry. The band structure was calculated along the K-path in reciprocal space: Γ(0,0,0)-H(0.5,-0.5,0.5)-N(0,0,0.5)-Γ(0,0,0)-P(0.25,0.25,0.25)-H(0.5,-0.5,0.5), and the partial density of states (PDOS) was also calculctaed.[2] Based on the expression $\frac{1}{m^*} = \frac{1}{h^2}\frac{d^2E}{dK^2}$, the

electron effective mass was calculated.

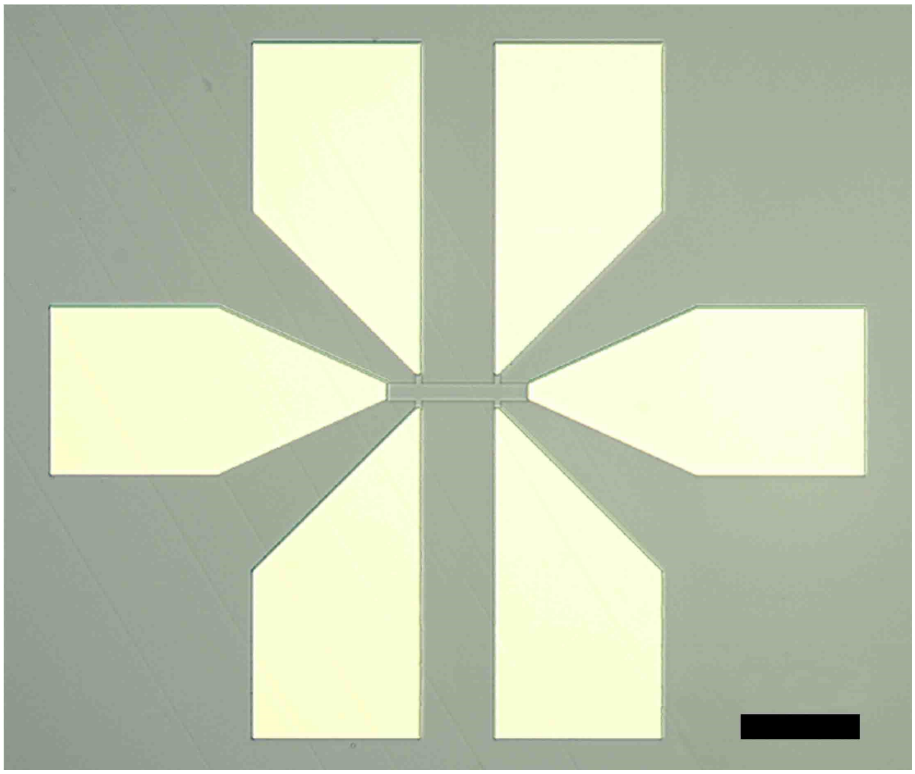

Figure S1. Optical image of the Hall bar. Scal bar, 200 μm.

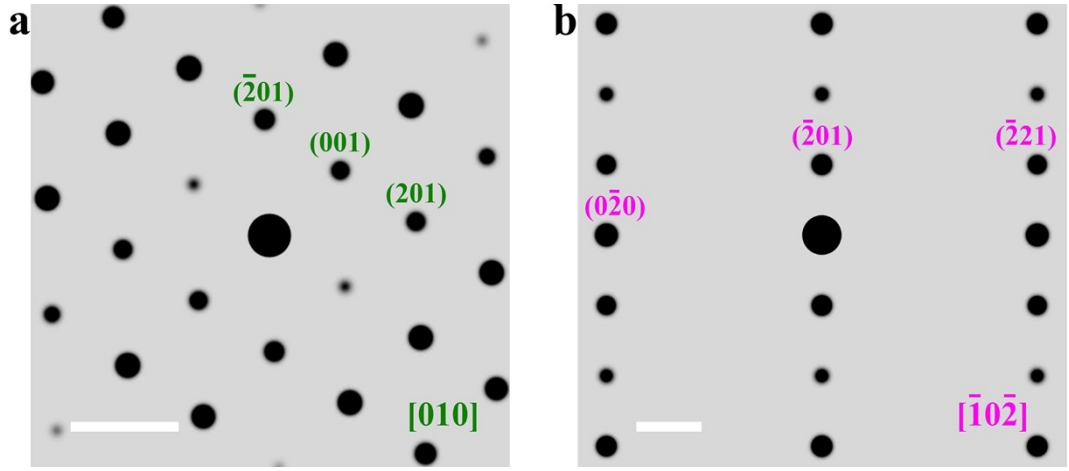

Figure S2. Simulated electron diffraction patterns of β-Ga_2O_3. (a) along [010] zone axis. Scale bar, 0.2 $Å^{-1}$. (b) along $[\bar{1}0\bar{2}]$ zone axis. Scale bar, 0.2 $Å^{-1}$.

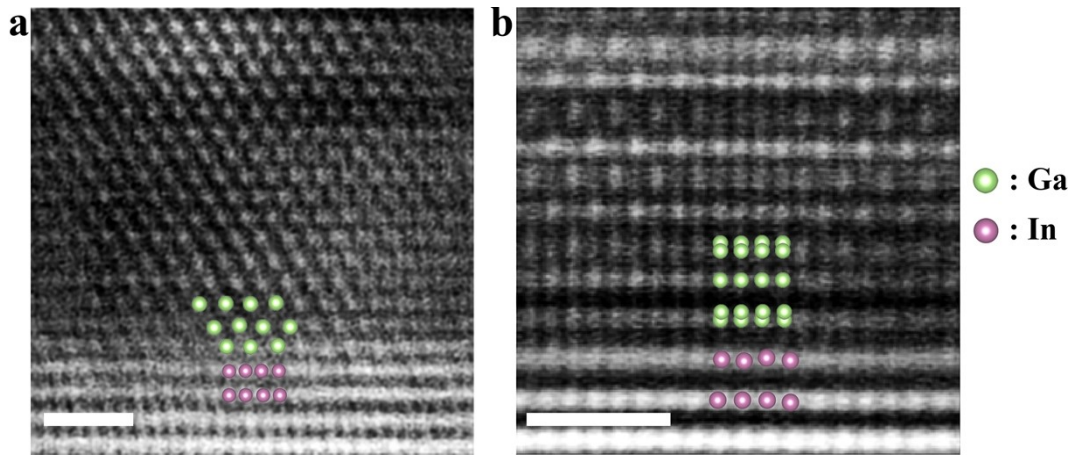

Figure S3. Interfacial HAADF images of Ga_2O_3/In_2O_3. (a) along [010] zone axis of β-Ga_2O_3. Scale bar, 1 nm. (b) along $[\bar{1}0\bar{2}]$ zone axis of β-Ga_2O_3. Scale bar, 1 nm.

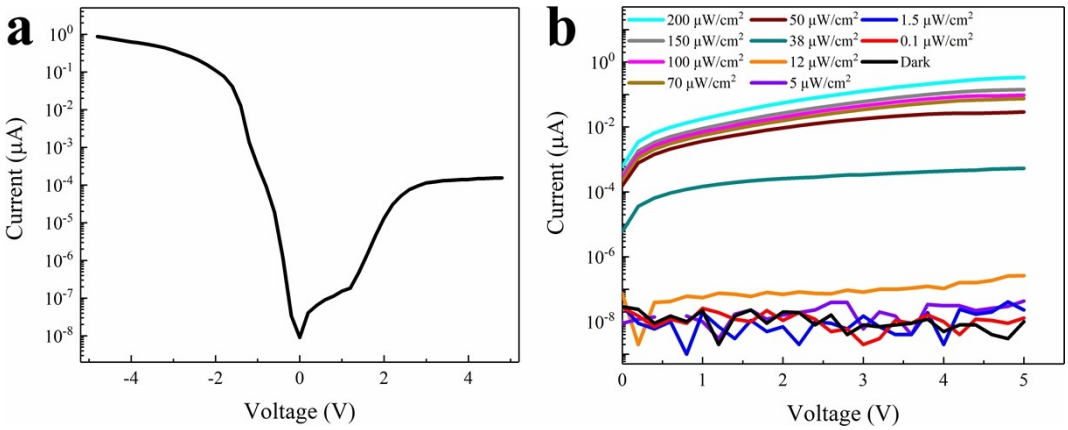

Figure S4. The I–V curve of the PDs. (a) With 20-nm-thickness a-In_2O_3 and 15-nm-thickness Ga_2O_3 under dark conditions. (b) With 5-nm-thickness a-In_2O_3 and 100-nm-thickness Ga_2O_3 under 254 nm illumination with different intensities.

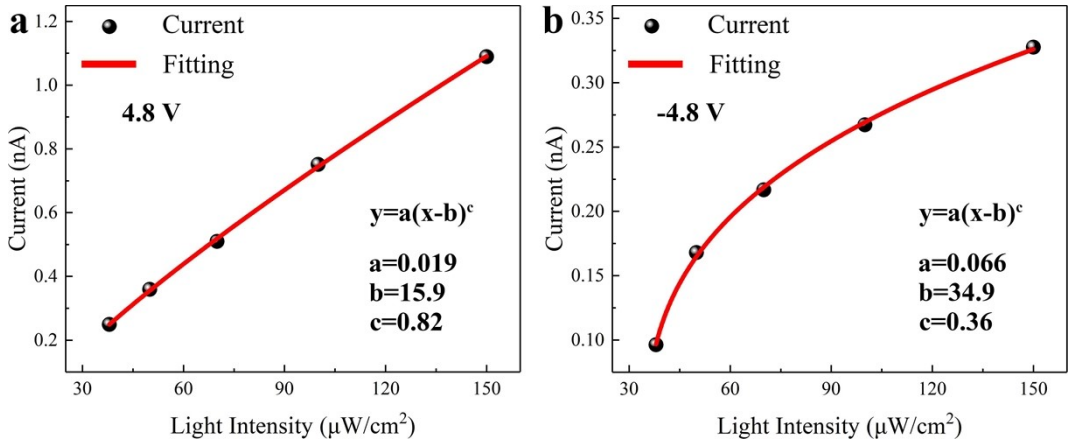

Figure S5. Photocurrent as a function of incident light power intensity under 254 nm light illumination. (a) At 4.8 V bias. (b) At -4.8 V bias.

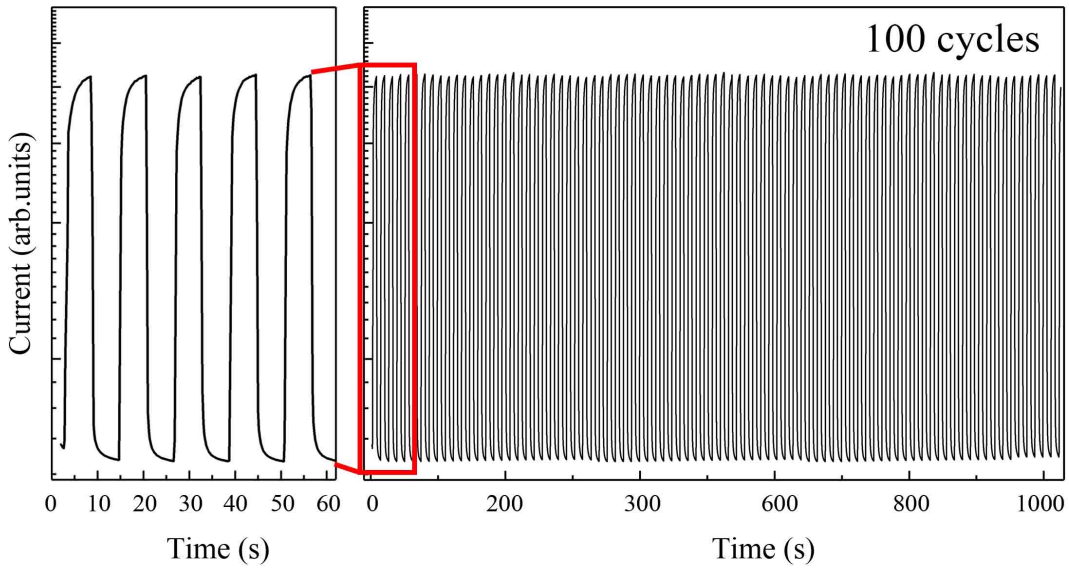

Figure S6. Stability and reliability characteristics of the PD through 10^2 On/Off cycles.

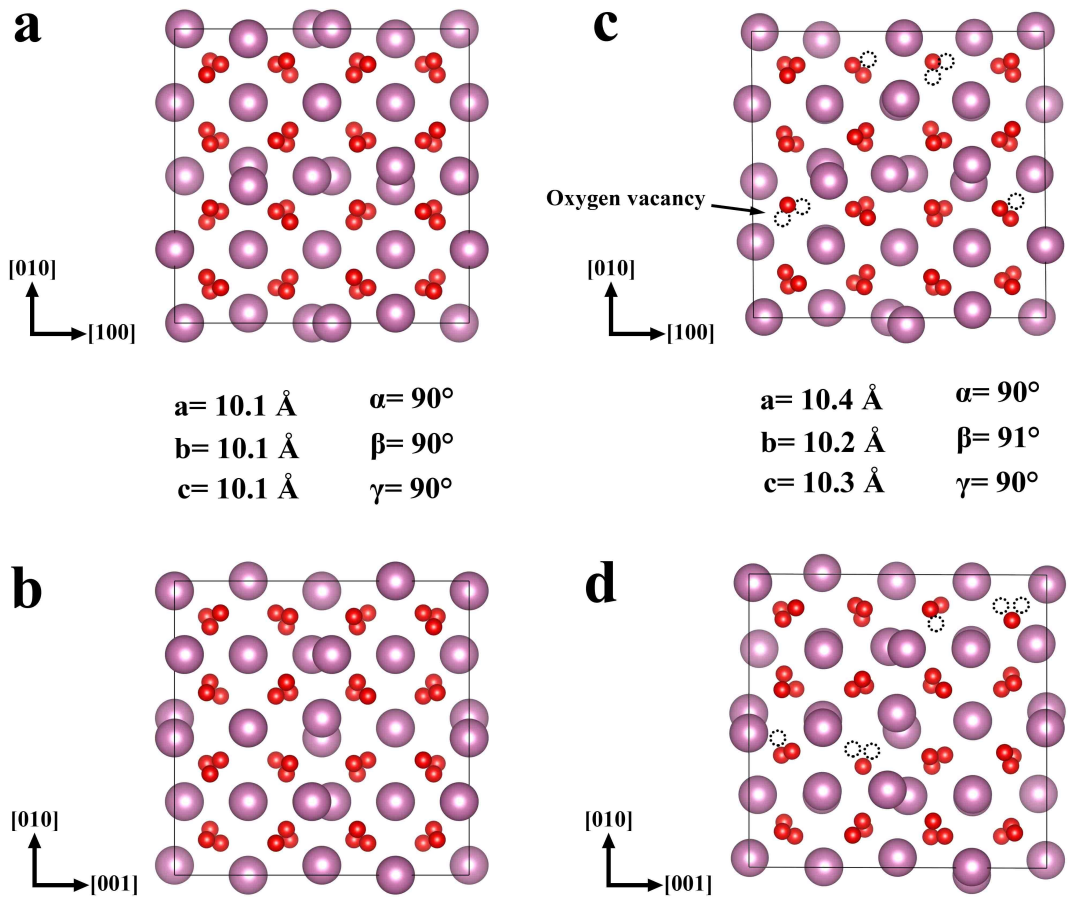

Figure S7. Schematic diagram of the structure model of the In_2O_3 used for DFT calculation. (a and b) The structure model of the In_2O_3 without oxygen vacancy along the view direction of [00 $\bar{1}$] and [100], respectively. (c and d) The structure model of the In_2O_3 with 10% oxygen vacancies along the view direction of [00$\bar{1}$] and [100], respectively. Black dotted circle represent oxygen vacancy. The oxygen vacancies results in a slight variation of lattice parameter of In_2O_3 structure.

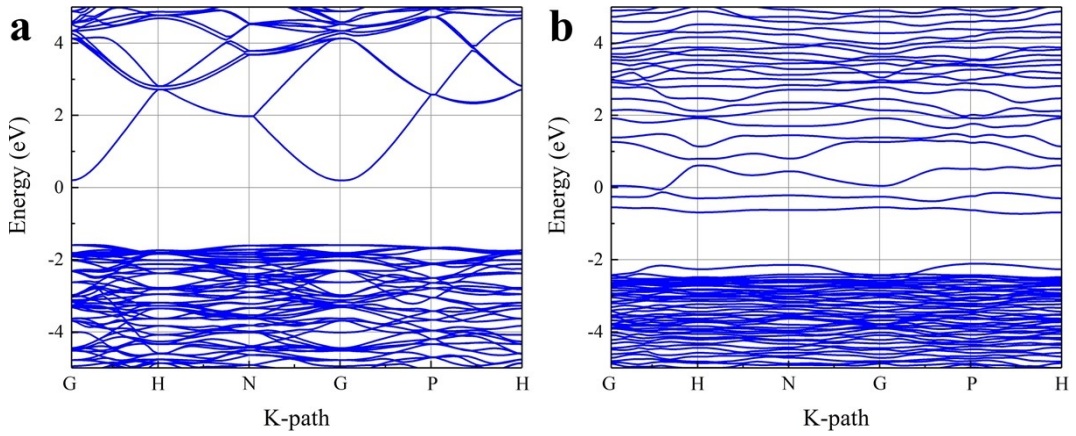

Figure S8. Energy band structure of In_2O_3 supercell. (a) Without oxygen vacancy. (b) With 10% oxygen vacancies. All Fermi levels in the patterns were set to zero.

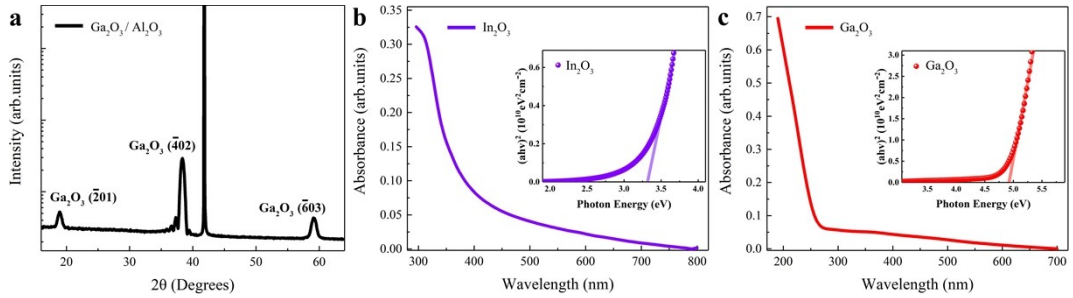

Figure S9. Structure and ultraviolet-visible (UV-vis) absorption spectrum of each layer. (a) XRD patterns of Ga_2O_3 grown on (0001) Al_2O_3 substrates. The Ga_2O_3 present C2/m phase. (b and c) UV-vis absorption spectrum with wavelength for Ga_2O_3 and In_2O_3 layers, respectively. The corresponding bandgap is shown in the inset.

The corresponding bandgap is shown in the inset. The direct bandgap of can be derived from the following function :[3]

$$(ahv)^2 = A(hv - E_g)$$

Where α is the absorption coefficient; h is Planck constant; v is the light frequency; A is a constant; Eg is the bandgap of the sample.

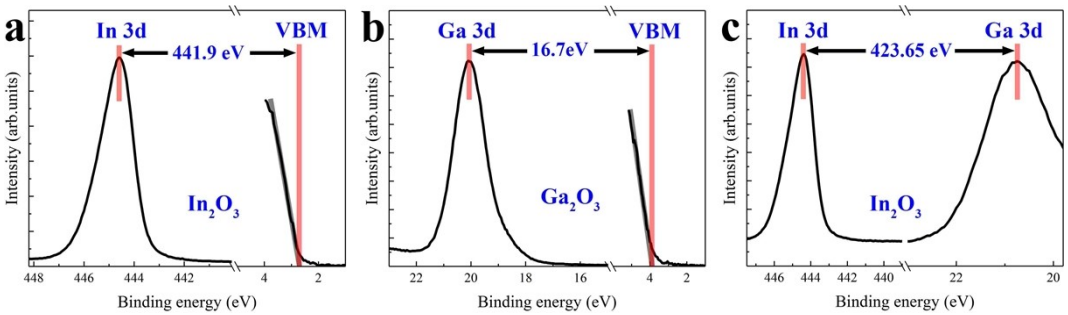

Figure S10. XPS measurements of In_2O_3/Ga_2O_3 heterostructure. (a) In 3d core level and valence band spectra of In_2O_3 bulk. (b) Ga 3d core level and valence band spectra of Ga_2O_3 bulk. (c) Ga 3d and In 3d core-level spectra of the Ga_2O_3 (2 nm)/ In_2O_3 (5 nm) sampl

Supplemental References

1 E. A. Kraut, R. W. Grant, J. R. Waldrop and S. P. Eowalczyk, Precise Determination of the Valence-Band Edge in X-Ray Photoemission Spectra: Application to Measurement of Semiconductor Interface Potentials, *Phys. Rev. Lett.*, 1980, **44**, 1620-1623.

2 P. E. Blochl, Projector augmented-wave method, *Phys. Rev. B*, 1994, **50**,

3 Y. H. Wang, W. J. Cui, J. Yu, Y. S. Zhi, H. R. Li, Z. Y. Hu, X. H. Sang, E. J. Guo, W. H. Tang and Z. P. Wu, One-Step Growth of Amorphous/Crystalline Ga_2O_3 Phase Junctions for High-Performance Solar-Blind Photodetection, *ACS Appl. Mater. Interfaces*, 2019, **11**, 45922−45929.